B

Insulating Biomaterials

Third Quarterly Progress Report
April-June, 1997

Submitted to:

Neural Prosthesis Program
National Institutes of Health
National Institute of Neurological
Disorders and Stroke

By the:

Biomedical Microelectronics Laboratory
Biomedical Engineering Center, Massachusetts Institute of Technology
West Roxbury VA Medical Center

Contributors:

David J. Edell, PI
Karen K. Gleason, Chemical Engineering
Bruce C. Larson, Grad Student, Electrical Engineering
Scott Limb, Grad Student, Chemical Engineering
James R. Mann, Electrical Engineering
Terry Herndon
Sean Sexton, Electronics
Cynthia M. Vanaria, Assembly

1. Instrumentation

1.1. High Temperature Soak System Instrumentation

The first assembly of 64 electrometers was completed this quarter. Software modifications were also completed to allow continuous measurements of 64 devices. 16 calibration plugs each with 4 calibration resistors were assembled and calibrated using a Keithley 617 electrometer. These calibration plugs were then used to calibrate the assembly of 64 electrometers. All electrometers were within 10% of the design specification.

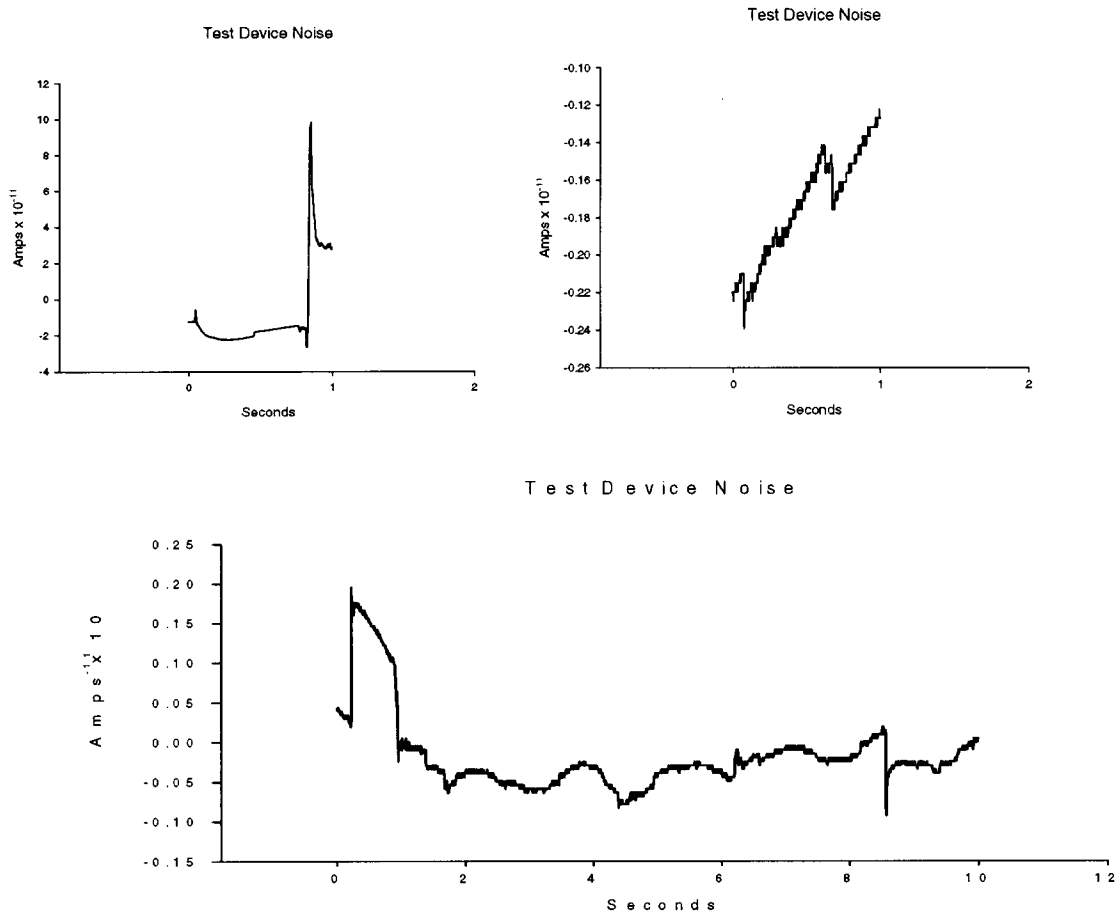

Figure 1: **Examples of raw data acquired from test devices under 90°C soak.**

16 long tubes with 64 devices that had been previously assembled and tested for the past year were attached to the new instrumentation. During testing, it was noted that the standard deviations of the measurements were quite high. By observing the raw data as acquired, it became apparent that there was substantially more noise in the measurements than that observed during the calibration. An example of the noise observed is shown in Figure 1. After a thorough review and investigation of the

grounding and shielding of the system, it was apparent that the noise was not due to the measurement system, but rather was an intrinsic property of the devices under test. Since this phenomenon was not observed with these test devices in the existing single electrometer system, further investigation of physical sources of noise was undertaken. Air currents, table vibration, temperature induced flexing of the leads from the electrometers to the test devices, subsonic pressure disturbances, and probably others were all considered. During these investigations, it was determined that the source of the noise was eliminated when the devices were allowed to cool to room temperature. The effect was repeatable, and not related to the heater itself. Apparently, it is the condensation of the water vapor that somehow was inducing the noise. Perhaps, during evaporation of the water, charge is lifted up into the tube. As the vapor condenses, droplets are formed on the walls of the tubes and wires leading to the devices at the bottom of the tube. The falling of these droplets apparently causes charge re-distribution in the wires that in turn causes large fluctuations in the measured current. When the effect is large enough, the input amplifiers saturate.

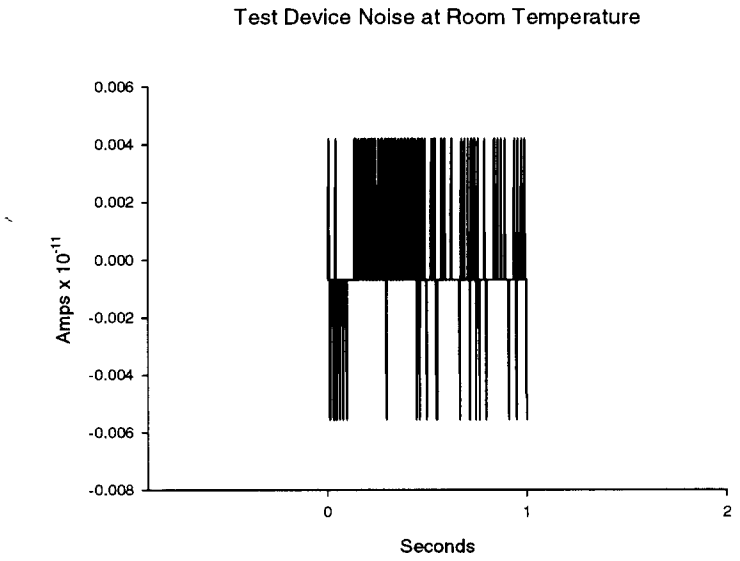

Figure 2: Raw data for a 1 second measurement of the same test device shown in Figure 1.

In the cases where saturation of the amplifiers occurs, a net DC offset is effectively induced which causes considerable measurement error. Though longer averaging times could reduce the error somewhat, in order to make measurements at least once per week, significantly longer averaging was not practical. Also, because of the unidirectional nature of the error, averaging is not as effective as when the glitches are AC coupled. Another technique for dealing with amplifier saturation would be to reduce the overall sensitivity of the system. This would allow averaging to further reduce the noise and thus would regain some sensitivity, but again the measurement times would be long. Since part of the accelerated testing protocol is to make the most sensitive

measurements possible to maximize detection of subtle trends, this alternative was also unattractive.

A third alternative was to electronically filter the signals. Electronic filtering can work well when the input amplifier does not saturate. A possible way to accomplish this would be to filter the input directly. This could be accomplished by adding a capacitor in parallel with the feedback resistor on the input amplifier. By choosing a reasonable time constant that was long enough to eliminate noise induced saturation of the amplifiers and short enough to allow measurements within one week, it might be possible to gain an order of magnitude or more in measurement sensitivity. The difficulty with this approach was that the parallel resistance associated with the feedback capacitors had to have a small voltage coefficient and be of higher value than the feedback resistors themselves. It was also important that the capacitors exhibit minimal long-term charge trapping. Polystyrene capacitors were most suited to this application. When we finally found some, we learned that the polystyrene film maker (Dupont), had discontinued the product and only existing stock would be available. Fortunately we found just enough at a west coast facility and have ordered them. In the mean time, we were able to borrow a few to verify our convictions.

Figure 3 shows a 1 second data grab during a transient disturbance. Compared to Figure 1, the transient is markedly suppressed. The amplifiers do not saturate with the filter in place which allows averaging to improve the data.

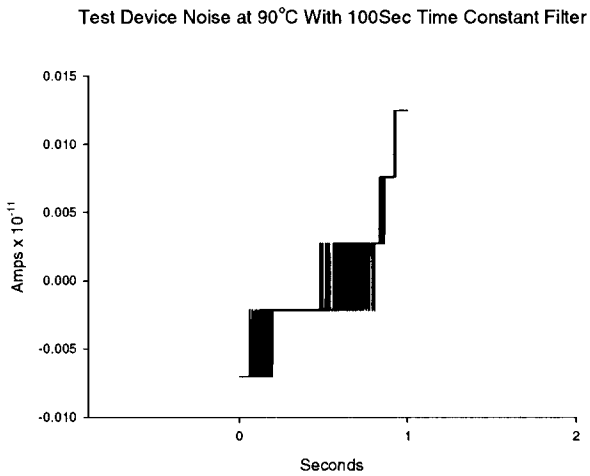

Figure 3: Same device at 90°C after installing 100sec time constant filter on input stage. Note excursion apparently caused by water droplet.

Figure 4 illustrates improvement of data with the filter in place over non-filtered data. The standard deviation of the mean of blocks of 600 samples was 0.51 without filtering and 0.28 with filtering. More aggressive filtering could be used if larger capacitors were available and longer measurement times were used, but the capacitors are not available and substantially longer times would be counterproductive.

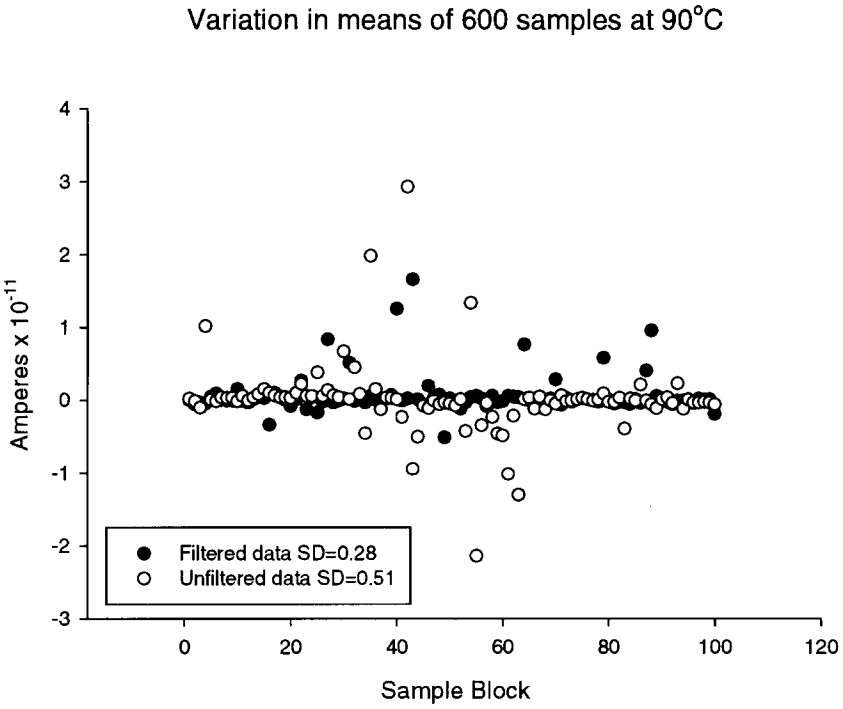

Figure 4: Variation of means of blocks of 600 samples taken from measurements of device under soak at 90°C with and without 100sec filter.

1.2. Current Description of Multichannel Electrometer System

The passivation materials high temperature soak test system provides the capability to simultaneously and continuously test up to 384 devices under saline soak. At this time, three different heater blocks will be used, at temperatures of 30°C, 60°C, and 90°C. Each heater block will hold up to 32 test tubes, each of which contains four test devices (for a total of 128 devices per heater block).

Every test tube has a standardized cable that connects it to a custom-built circuit board that biases its soak solution to a set voltage and measures the leakage currents of the four test devices it contains. These electrometer circuit boards are placed into boxes of 16 that are situated on either side of the heater blocks. Another custom printed circuit "patch board" in each box interfaces the electrometer boards to a Data Translation, Inc. DT727 channel expansion board that is used to multiplex the 64 leakage current measurement channels of the box to a single output.

Testing is performed by a Windows 95 PC. A Data Translation, Inc. DT31-EZ data acquisition board in the PC provides the interface to the six electrometer boxes via a daisy-chain cable connecting it to the patch boards in the boxes. On the DT31-EZ, the digital port is used to address the desired leakage current measurement channel, one of its digital-to-analog converters generates the bias voltage signal, six of its 16 analog-to-digital converter inputs are used to verify the bias in each box, and six more of its

analog inputs sample the selected measurement channel of each box. The remaining four analog inputs of the DT31-EZ will eventually monitor the ambient humidity in the room and the temperatures of the three heater blocks.

An application developed with Hewlett-Packard's HP-VEE software automates the testing. This program sets the bias voltage on the devices according to a user-defined sequence, waits a specified amount of time for the measurement to settle, and then takes a user-specified number of samples for each of the devices under test. The electrometer current-to-voltage converter circuits have been re-designed with a 100-second time constant low-pass filter (1.6 milliHertz) to the smooth the data and average out transients due to motion and condensation in the tubes. In order to have statistically useful samples, they must be taken more than 100 seconds apart in time. By using the averaging of 600 measurements taken at 600 Hz to make a single sample, it takes the system approximately two minutes to address and sample all 384 devices (only 64 seconds are required for the actual measurements because six devices, one from each box, are sampled simultaneously). So no additional delay is needed between the samples. When the required number of samples at the bias voltage have been taken, the mean and standard deviation of the leakage current of each device are saved to a file. The bias voltage is changed to the next value in the sequence, and the system again waits for the settling time.

Presently, an 84 point voltage sweep going from 0V to +5V, down to -5V, and back to 0V is being used for the testing. The sweep has a higher density of bias points between ±0.5V in order to get more accurate testing of devices with lower insulation resistances. Out of range (saturated) samples are ignored, so that devices of widely ranging resistances may be measured with this biasing technique. When a sweep is completed, the test program calculates the resistance of each device by fitting a line to the I-V data collected for the sweep. This resistance is appended to a log file for the device and also stored in a summary file containing only the most recent resistances of all devices under test. Thus convenient summary information is provided in addition to the continuous log of raw leakage current / bias voltage data for each device. Unless the program is interrupted, a new sweep is started and the process continues. With a 30 minute settling time between bias points, it takes approximately 50 hours to complete one sweep.

The current-to-voltage conversion factor of 80 of the 96 electrometer boards was designed to be 10^{12} Ω, in order to measure resistances between about 10^{9} Ω and 10^{15} Ω. The other 16 electrometer boards were built with a transimpedance of 10^{11} Ω to measure resistances from about 10^{8} Ω to 10^{14} Ω.

The system will become operational next quarter when the feedback capacitors are installed on the electrometer boards.

1.3. Improved Instrumentation for Animal Measurements

The electrometer head stage constructed this quarter was successful in reducing motion artifact to a minimum. However, in spite of careful grounding procedures, the inputs to several of the LMC660 quad electrometers failed. Apparently, the fur is to blame. Also, apparently the Analog Devices 549 electrometer op-amps are more

robust. An alternative approach, developed based on our experience with the high temperature system is to use parallel capacitors on the electrometer feedback resistors. A test of this approach showed that the motion artifacts were substantially reduced. In addition, $10^8\Omega$ resistors were added in series with the electrometer inputs. The thought is that the series resistance will limit current flow onto the feedback capacitor thereby protecting the inputs to the electrometers without compromising the measurements.

2. Surface Interface Protection

A new triple track device that was assembled using Nusil Med-4-4220 silicone is showing encouraging results at the 10^{12}-$10^{13}\Omega$ level at 90°C. This material is easy to handle, comes in side by side cartridges for ease of dispensing, and is medical grade. If the soak tests warrant, subdural animal implants will be fabricated next quarter.

3. Wire Insulation

Wire loops of PFA Teflon have been fabricated and implanted in animals as detailed below. Fluorocarbon wires have been assembled into new test structures that require only 2cm of good wire. The problems in the past were often related to the small size of the uniform deposition zone in our experimental reactor. By trying to use too long a length of wire, portions of the wire that were not well coated were often exposed to the saline. The new structure also requires minimal handling and flexing of the wire. Basically, the wire holder is now a simple drum of silicone coated glass. The extension wires are pre-assembled to the drum. When the test wires are added, they are simply placed around the drum, fixed in place, and soldered to the extension wires. The extension wire joint is then covered with silicone so the only area exposed to the saline is from the best portion of the wire. Fluorocarbon coated wires assembled this way are performing well.

Silicone coated wires are anticipated next quarter. If reactor coated silicone works, it may be possible to at last achieve a one component coating that will allow thin film coating of the silicon substrate, bond area, and lead wires.

4. Fluorocarbon Research

Several sets of wire loops coated with PECVD fluoropolymer have been placed under soak and some are exhibiting encouragingly low leakage currents. Defects/pinholes in the films are a significant problem at present. During these coating runs, we learned that the plasma environment was etching platinum wires. Further investigation of how to protect the platinum from the reactive fluorine gas will be undertaken next quarter. Stainless steel and copper, however, do not appear to be attacked as aggressively as the platinum. Another set of wires will be coated and perhaps used for animal implants if the soak tests are successful. A paper comparing PECVD fluoropolymer to thermally decomposed hexafluoropropylene oxide is appended to this progress report.

5. Thermal Silicone Research

Basic work on deposition of silicones from thermal decomposition of monomer gases is underway. Silicon substrates will be coated and tested for insulation properties using the surface coating test protocol. This involves insulating the sides and backs of the silicone substrates with Nusil CF20-2186 and testing the resistance through a $1cm^2$ area of the film under test. If this test shows promising results, the deposition procedure will be applied to wires and triple track devices as well. The first devices will be put under test next quarter.

6. Animal Implants

Wire loop test devices were fabricated and implanted this quarter. The connector used for these devices was Microtech's Teflon® insulated 12 pin connectors. Epoxy Technology 353 was used to insulate the solder joints and Teflon® interface of the connector. By completely wrapping the bottom of the connector with 353, and burying the epoxy in the acrylic used for the head mount, it was hoped that sufficient insulation for high impedance readings would be achieved. The exposed area of the 2mil diameter platinum wire was approximately 2cm long and was slipped under the dura over the right parietal cortex. Carboxylate cement (Durelon®) was used to interface the acrylic to the bone. Anchor holes for the carboxylate cement were drilled and filled with the cement prior to application of the acrylic. 3M DP805 acrylic adhesive was used to anchor the 353 of the connector to the carboxylate cement. Carboxylate cement was also used to repair the skull defect and to coat the lead wires between the connector and the dura.

New Molex connectors insulated with Epoxy Technology 353 and 377 arrived from the University of Michigan and have been placed under soak. Microtech connectors insulated with 353 and 377 have also been placed under soak.

Triple track animal implants will be constructed with Med-4-4220 and implanted subdurally next quarter.

7. Flexible Circuit Materials Evaluation

After rapid failure of most Kapton® based flexible circuit encapsulation test electrodes, a simpler test was devised which consists of coating a single ribbon cable with the material under test and then immersing it in saline through the top of a small jar. The ribbon is sealed into the jar with RTV silicone.

Measurements are simply manually hooking up the electrometer, setting the bias, and waiting an hour or so for slow charge traps to fill/empty. Readings are done at 2 bias points, ±10 volts. Effective resistances less than $10^6\Omega$ are probably indicative of failures for this application where overall shunt resistances should be greater than $10^7\Omega$. Since the University of Michigan Kapton® cables have a much smaller shunt resistance path, encapsulants on these test devices that maintain greater than $10^6\Omega$ should be sufficient. Also, so far, devices that exhibit high leakage current also show visible signs of corrosion of the interdigitated electrode arrays.

Thus far no strong recommendations regarding the various encapsulants can be made because data is too sparse. However, results of epoxies on Kapton® are encouraging. Silicone results are somewhat discouraging because this means that an epoxy-silicone interface will need to be used on the real devices.

Epotek 353 and 377 are very good epoxies that can withstand autoclave environments. Epotek 715 is a promising solution because it was designed for use with acrylics. Since the most common Kapton-copper material uses acrylic adhesive, use of an acrylic compatible epoxy seems appropriate.

Once a promising approach is identified, more assemblies will be constructed and placed under high temperature soak.

Number	Sample ID	Ribbon	Encapsulant Class	Encapsulant	Date 1st Saline	Initial Wet	Current Date	Current Read	Days Under Soak	Units
1	KTT16A-34	Bare Kapton	Silicone	CF20-2186	3/16/97	3.61E+04	5/25/97	3.45E+05	70	Ohms
2	-56		Silicone	CF20-2186	3/16/97	8.15E+07	5/25/97	9.26E+07	70	Ohms
3	-78		Silicone	CF20-2186	3/16/97	5.29E+07	5/25/97	5.91E+05	70	Ohms
4	-910		Silicone	CF20-2186	3/16/97	2.49E+07	5/25/97	2.88E+02	70	Ohms
5	KTT26A-34	Bare Kapton/Acrylic	Silicone	CF20-2186	3/17/97	5.51E+07	4/6/97	1.76E+03	20	Ohms
6	-56		Silicone	CF20-2186	3/17/97	1.26E+08	4/6/97	1.99E+08	20	Ohms
7	-78		Silicone	CF20-2186	3/17/97	3.17E+07	4/6/97	2.79E+02	20	Ohms
8	-910		Silicone	CF20-2186	3/17/97	7.80E+02	4/6/97	8.15E+03	20	Ohms
9	KTT3BA-34	Kapton/Acrylic Sand	None	None	3/23/97	5.56E+09	5/26/97	3.98E+03	64	Ohms
10	-56		None	None	3/23/97	8.40E+09	5/26/97	5.98E+03	64	Ohms
11	-78		None	None	3/23/97	8.46E+09	5/26/97	6.66E+03	64	Ohms
12	-910		None	None	3/23/97	4.58E+09	5/26/97	4.18E+03	64	Ohms
13	KTT5BA-34	Kapton/Epoxy	None	None	5/12/97	1.75E+06	5/28/97	2.07E+05	16	Ohms
14	-56		None	None	5/12/97	1.73E+06	5/28/97	1.35E+06	16	Ohms
15	-78		None	None	5/12/97	2.62E+05	5/28/97	1.42E+06	16	Ohms
16	-910		None	None	5/12/97	1.59E+06	5/28/97	1.28E+06	16	Ohms
17	KTT13A	Kapton	Epoxy	Epotek 353	5/13/97	1.20E-13	5/28/97	1.00E-09	15	Amps@10v
18	KTT17A	Kapton	Epoxy	Epotek 377	5/13/97	3.00E-13	5/28/97	3.20E-11	15	Amps@10v
19	KTT1GA	Kapton	Epoxy	Epotek 87-GT	6/2/97	5.00E-12	6/9/97	2.30E-08	7	Amps@10v
20	KTT25A	Kapton/Acrylic	Acrylic Epoxy	Epotek 715	6/4/97	2.00E-09	6/9/97	8.00E-09	5	Amps@10v
21	KTT25CA	Kapton/Acrylic	Acrylic Epoxy	Epotek 715	6/11/97	9.50E-08	6/11/97	9.50E-08	0	Amps@10v
22	KTT25CB	Kapton/Acrylic	Acrylic Epoxy	Epotek 716	6/13/97	1.30E-08	6/13/97	1.30E-07	0	Amps@10v
23	KTT28A	Kapton/Acrylic	Acrylic Adhesive	3M DP805	6/12/97	1.00E-04	6/14/97	3.00E-03	44	Amps@10v
24	KTT2GA	Kapton/Acrylic	Epoxy	Epotek 87-GT	6/10/97	2.70E-08	6/12/97	1.00E-04	2	Amps@10v
25	KTT3VA	Kapton/Acrylic Sand	Saline filled vial	None	5/6/97	8.00E-13	5/29/97	2.00E-12	23	Amps@10v
26	KTT43A	Kapton/Epoxy	Epoxy	Epotek 353	5/16/97	1.70E-08	5/29/97	6.90E-07	13	Amps@10v
27	KTT47A	Kapton/Epoxy	Epoxy	Epotek 377	5/16/97	2.90E-08	5/29/97	3.00E-06	13	Amps@10v

Figure 5: Summary of Kapton® interdigitated electrode test devices. All at room temperature except multi-device tubes which were at 90°C. Devices under bias only for measurements.

Comparison of Pulsed Plasma Enhanced Chemical Vapor Deposition and Pyrolytic Chemical Vapor Deposition from Hexafluoropropylene Oxide

Scott J. Limb[1], David J. Edell[2], Edward F. Gleason[3], and Karen K. Gleason[1*]

[1]Department of Chemical Engineering, MIT

Cambridge MA 02139

[2]Division of Health and Sciences, Harvard University

Cambridge MA 02139

[3]MIT Lincoln Laboratory
Lexington MA 02173

Introduction

Fluorocarbon thin films have numerous potential applications. These include biopassivation, low dielectric constant, and low friction coatings. Thus, there has been extensive research on the deposition of these materials.[1,2] The most commonly used technique is plasma-enhance chemical vapor deposition(PECVD). Despite the many process parameters associated with PECVD (precursor choice, applied rf power, gas flow rate, pressure, substrate temperature, etc.), it is difficult to vary the fluorocarbon film stoichiometry over a wide range. Typical PECVD films have F/C ratios of ~ 1.6 and CF_2 percentages of ~ 35%. Thus, alternate deposition methodologies are desired which enable

fluorocarbon film composition to be controlled over a wider range. In particular, films with high percentages of CF_2 are anticipated to have properties related to that of bulk polytetrafluoroethylene [PTFE, $(CF_2)_n$, Teflon™].

Films containing up to 90% CF_2 have been achieved using two different chemical vapor deposition (CVD) techniques. Pulsed PECVD allows long lived neutrals to dominate the deposition process during the off-time in between the applied rf pulses. Pulsing the plasma excitation also limits the exposure of the growing surface to ion bombardment.[3-5] In pyrolytic CVD, ion bombardment is entirely avoided. The gas-phase composition of the CVD chamber is also expected to depend on whether continuously applied rf, pulsed rf, or thermal energy is used to excite the homogeneous chemistry.[5] Both methods use hexafluoropropylene oxide (HFPO) as the precursor gas. Indeed, HFPO has been used as a clean source of CF_2 for surface chemistry studies.[4,6] Furthermore, the 31 kcal/mole activation energy for the production of difluorocarbene from HFPO was found to agree with the apparent activation energy for depositing pyrolytic CVD films with high percentages of CF_2.[7]

In this communication, we will compare the composition of pulsed PECVD and pyrolytic CVD films using x-ray photoelectron spectroscopy (XPS) and fourier transform infrared spectroscopy (FTIR). In addition, the degree of crystallinity and the crystal structure of these films will be examined using X-ray diffraction (XRD). Understanding differences in morphology, as well as stoichiometry, will aid the development of structure-property relationship for CVD fluorocarbon films.

Experimental

A single reactor was configured to carry out both the pulsed PECVD and pyrolytic CVD processes. Detailed descriptions of both types of experiments have been previously reported. [3,5 7] For this study, all films were deposited from undiluted HFPO(from PCR Inc., 99% purity). The silicon wafer substrates were maintained at 293 ± 3 K by backside water cooling. A reactor pressure of 1 torr and flow rate at 23 sccm (STP) were used. Pyrolytic CVD was accomplished using a hot-filament made by resistively heating Ni/Cr wire. The filament temperature (T_f) was 673 K. Substrates were placed on the grounded electrode and the peak applied rf(13.56 MHz) was set at 280 W. Pulsed on-time and off-time(ms/ms) of 10/20 and 10/400 were used.

Films were characterized by ellipsometry(λ=6328Å), X-ray photoelectron spectroscopy (XPS)(Perkin Elmer 5100, Mg anode), fourier transform infrared spectroscopy (FTIR)(Nicolet 860), and Cu Kα 2θ X-ray diffraction (XRD)(Rigaku Ru300). The deposited samples varied in thickness from 0.3 to 0.7 μm. Furthermore, for reference an XRD pattern was taken of as-polymerized PTFE powder. This bulk PTFE sample was at least 90% crystalline as determined from infrared spectroscopy and density calculations made by DuPont.

Results and Discussion

The XPS line shapes shown in Fig. 1 were deconvoluted in order to obtained the integrated areas of the CF_3, CF_2, CF, and C-CF components. The carbon 1s (C1s) binding energies of 294, 292.1, 289.5, and 287.3 eV were used for CF_3, CF_2, CF, and C-CF

(carbon with β substituted fluorine) species respectively.[1] Good correlation between the predicted and experimental XPS spectra of the films were obtained by assuming each component had a 60/40 Gaussian/Lorentzian line shape having a full width at half-maximum fixed at 2 eV. Also, the central binding energies were allowed to vary ± 0.2 eV for the CF_3, CF, and C-CF components while keeping the others fixed.

For a pyrolytic CVD deposited film(Fig. 1a), the dominate CF_2 peak at 292 eV comprises 90% of the total area. The other peaks, representing CF_3 and CF, comprise 5% each of the total area and, interestingly, no C-CF component is seen. For the pulsed PECVD films, the highest $\%CF_2$ film corresponds to a 10/400 ms-on/ms-off condition(Fig. 1b). For this film, the CF_2 peak at 292 eV accounted for 62% of the total area of the C1s XPS spectra. The percentages of CF_3 and CF, 15% and 11% respectively, are higher than in the pyrolytic CVD film. Also, 12% of the area in the 10/400 pulsed PECVD XPS spectra is associated with the C-CF feature, which was undetectable in the pyrolytic CVD film(Fig. 1a). Furthermore, for the film deposited at 10/20 ms-on/ms-off condition, the spectra(Fig. 1c) displays even more intensity in the non-CF_2 components(19% CF_3, 23% CF_2, 29% C-CF). Thus the CF_2 component accounts for only 39% of the total area. The comparison of these XPS spectra shows that the degree of crosslinking(CF and C-CF components) can be controlled over a wide range using pyrolytic CVD and pulsed PECVD.

For all pyrolytic CVD and pulsed PECVD films, XPS survey scans show that the oxygen content were less than 2 atomic%. Some or all of this oxygen may result from the films' exposure to atmospheric conditions. Also, note that contributions at 285 eV from

carbon with no β substituted fluorine are below the detection limit in all the spectra in Fig. 1. Thus, contamination from extraneous hydrocarbon species is negligible.

From XPS spectra, the pyrolytic CVD process deposited films closest in composition to bulk PTFE. The advantage of this pyrolytic CVD process is the absence of surface defluorinating species which can arise in a plasma. In a plasma, ions,[8] X-rays,[9] electrons,[10] and fluorine atoms[11] are all capable of altering the surface of bulk PTFE and lowering the CF_2 fraction, and can also presumably have the same effect on CVD fluorocarbon films. Furthermore, gas-phase composition of film forming species may be comprised of a high CF_2 concentration due to HFPO thermally decomposing into a difluorocarbene, CF_2, and a stable carbonyl,[12] allowing the highest $\%CF_2$ content films to be deposited from pyrolytic CVD.

On the other hand, plasma excitation from HFPO can, not only produce CF_2 in the gas-phase,[12] but can also form non-CF_2 film forming species from the glow discharge. Thus, pulsing the plasma excitation would effect both gas-phase chemistry and plasma interaction with the surface.[5] For the 10/400 ms-on/ms-off condition higher $\%CF_2$ deposited films were attained compared to the 10/20 ms-on/ms-off condition. This shows that CF_2 gas-phase fraction increases and/or surface defluorination decreases as duty cycle ($t_{on}/(t_{on} + t_{off})$) is decreased.

Shown in Fig. 2 is a comparison of the FTIR spectra of a pyrolytic CVD film and two pulsed PECVD films(10/400 and 10/20 ms-on/ms-off). The CF_x bands fall in the region 980-1450 cm^{-1} and have been assigned using a compilation developed for PTFE and

conventional PECVD materials.[1] For the pyrolytic CVD film(Fig. 2a), the symmetric(1160 cm^{-1}) and asymmetric(1220 cm^{-1}) CF_2 stretches are sharp and can be clearly resolved. The only other significant feature in Fig. 2a is a weaker absorption at around 650 cm^{-1}, representing CF_2 wagging modes. Thus, the FTIR results(Fig. 2a) confirm the XPS findings(Fig. 1a) that the pyrolytic CVD films are composed predominately of CF_2.

In the FTIR spectra of the 10/400 film (Fig. 2a), the CF_2 symmetric and asymmetric stretches are again predominate. However, the bands are broader and overlap with other features, such as a CF stretch centered at 1340 cm^{-1} and thus are not as distinctly resolved. Fig. 2b also shows two weak absorptions not seen in Fig 2a. One is a CF_3 band at 980 cm^{-1}. The second is around 740 cm^{-1} and may arise from chain disorder[13] and thus may indicate amorphous regions in the film.

In the FTIR spectra of the 10/20 film(Fig. 2c), the symmetric and asymmetric CF_2 stretches are no longer resolvable. This indicates a higher degree of disorder in the film resulting in line broadening and increased overlap with absorptions from non-CF_2 moieties. The CF_3 and "amorphous" PTFE modes, are stronger than those observed in Fig 2b. Also, in Fig. 2c, there is a broad weak absorption between 1650 and 1800 cm^{-1} most likely arising from C=O (1720 cm^{-1}) and/or C=C (1780 cm^{-1}). Figs. 2a and 2b also show a hint of intensity in this region but in Fig. 2c it is more pronounced.

Diffraction pattern of an as-polymerized PTFE powder(Fig. 3a) is compared to those for the pyrolytic CVD (Fig. 3b), 10/400 pulsed PECVD (Fig. 3c), and 10/20 pulsed PECVD(Fig. 3d) films. Fig. 3a for the as-polymerized PTFE sample is dominated by a

sharp diffraction peak at a 2θ value of 18.0°. This feature corresponds to the {100} plane of the hexagonal structure with a d-spacing of 0.4992 Å.[14,15] Crystalline PTFE above 19 °C has an hexagonal unit cell with lattice parameters of a=0.566 nm and c=1.95 nm.[16] This represents a repeat unit having 15 CF_2 groups. Fig. 3b also shows a diffraction peak at 2θ = 18.0°. This indicates the hexagonal phase found in the bulk PTFE at room temperature also occurs in the pyrolytic CVD film. However, the linewidth of the 18.0° peak is significantly broader in Fig. 3b than in Fig. 3a. This suggest average crystallite sizes in the film are smaller than in the bulk polymer.

Also, the less intense diffraction peaks at 32°, 37°, and 41° in the patterns from the bulk PTFE are not detectable in Fig. 3b. This could indicate the pyrolytic CVD film has a fiber texture with the (100) chain axis parallel to the substrate. This result was also reported for films produced by pulsed-laser deposition and ion-assisted evaporation of PTFE. [14,15] However, in the case of Fig. 3b an alternate interpretation is possible. The overall intensity of diffraction is low, as evidence by the visible noise level. If in addition, there is line broadening, the other diffraction peaks could simply fall below the detection limit even if the crystallites in the film are isotropically orientated. Additional work would be required to conclude whether or not partial orientation of the crystalline regions in the pyrolytic CVD film exists.

The diffraction patterns(Figs. 3c and 3d) of the pulsed PECVD films did not show any detectable sharp peaks at 18.0°. Instead, for the 10/400 pulsed PECVD film, the

presence of a broad peak at 16.1° may represent an overlap of the crystalline peak at 18.0° with an amorphous halo.

A relationship between composition and degree of crystallinity is seen. As the degree of crosslinking increased, the crystalline region in the films decreased. This observation can be attributed to the number of CF_2 units needed to form a crystalline unit cell and the mobility of these CF_2 units. It is expected that as the fraction of CF_2 in the film decreases, the probability of having 15 CF_2 units to form a hexagonal unit cell decreases. Furthermore, due to crosslinking units, the decreased mobility is expected to hinder the ability of a CF_2 unit to configure itself into a crystalline state.

In conclusion, deposition from HFPO under pyrolytic CVD, pulsed and continuous PECVD conditions resulted in different degrees of CF_2 incorporation in the films. The highest $\%CF_2$ content was deposited from pyrolytic CVD making it a promising method for depositing fluorocarbon polymer films with chemical resemblance to bulk PTFE. Furthermore, pyrolytic CVD films were found to be more crystalline as compared to the pulsed PECVD counterparts. Amorphous regions in the pulsed PECVD films could be observed by FTIR and XRD. The increased amorphous nature of the pulsed PECVD films may be attributed to significant concentrations of CF_3, CF, and C-CF species which destroy the ability of the structure to order and potentially to the disorder induced by ion bombardment during the deposition process. The presence of CF_3, CF, and C-CF units may lessen the tendency for CF_2 units to crystallize and thus composition can be used to control the degree of crystallinity.

Acknowledgment

We wish to gratefully acknowledge the NIH for support of this work under Contract N01-NS-3-2301 and the NSF for support by CTS-9057119. We would also like to acknowledge Russell Negin for collecting the XRD patterns.

References

(1) d'Agostino, R.; Cramarossa, F.; Fracassis, F. ;Illuzzi, F. In *Plasma Deposition Treatment, and Etching of Polymers*, edited by d'Agostino, R.; Academic Press, San Diego, 1990; pg 95.

(2) Yasuda, H. *Plasma Polymerization*, ; Academic Press: Orlando, 1985.

(3) Limb, S. J.; Gleason, K. K.; Edell, D. J. ;Gleason, E. F. *J. Vac. Sci. Technol.* **1997**, *A15,* August.

(4) Savage, C. R.; Timmons, R. B. ;Lin, J. W. *Adv. Chem. Ser.* **1993**, *236,* 745.

(5) Limb, S. J.; Edell, D. J.; Gleason, E. F. ;Gleason, K. K. *Submitted to Chemistry of Materials* **1997**.

(6) Gray, D. C. ;Sawin, H. H. *J. Vac. Sci. Technol.* **1991**, *A9,* 779.

(7) Limb, S. J.; Labelle, C. B.; Gleason, K. K.; Edell, D. J. ;Gleason, E. F. *Appl. Phys. Lett.* **1996**, *68,* 2810.

(8) Wells, R. K.; Ryan, M. E. ;Badyal, J. P. S. *J. Phys. Chem.* **1993**, *97,* 12879.

(9) Wheeler, D. R. ;Pepper, S. V. *J. Vac. Sci. Technol.* **1982**, *20,* 226.

(10) Clark, D. T. ;Brennan, W. J. *J. of Elect. Spect. and Rel. Phenon* **1986**, *41,* 399.

(11) d'Agostino, R.; Cramarossa, F. ;Illuzzi, F. *J. Appl. Phys.* **1987**, *61,* 2754.

(12) Knickelbein, M. B.; Webb, D. A. ;Grant, E. R. *Mat. Res. Soc. Symp. Proc.* **1985**, *38,* 23.

(13) Fisher, W. K. ;Corelli, J. C. *J. Polym. Sci.: Polym. Chem. Ed.* **1981**, *19,* 2465.

(14) Usui, H.; Koshikawa, H. ;Tanaka, K. *J. of Vac. Sc. Technol.* **1995**, *A13,* 2318.

(15) Jiang, W.; Norton, M. G.; Tsung, L. ;Dickinson, J. T. *J. Mater. Res.* **1995**, *10,* 1038.

(16) Clark, E. S. ;Muus, L. T. *Z. Kristallogr. B.* **1962**, *117,* 119.

Figure Captions

Figure 1. Carbon 1s XPS spectra of (a) pyrolytic CVD film, (b) 10/400 ms-on/ms-off pulsed PECVD film, and (c) 10/20 ms-on/ms-off pulsed PECVD film. For each, the best fit spectra and four components from the deconvolutions are also shown. XPS survey scans show the oxygen content to be less than 2%.

Figure 2. FTIR absorbance spectra of (a) pyrolytic CVD films, (b) 10/400 ms-on/ms-off pulsed PECVD film, and (c) 10/20 ms-on/ms-off pulsed PECVD film. The CF_2 symmetric and asymmetric stretches are clearly resolved in the pyrolytic CVD and 10/400 pulsed PECVD spectra.

Figure 3. X-ray diffraction patterns for (a) as-polymerized PTFE powder, (b) pyrolytic CVD film, (c) 10/400 ms-on/ms-off Pulsed PECVD film and (d) 10/20 ms-on/ms-off Pulsed PECVD film. The sharp crystalline peak for the (100) plane of hexagonal PTFE occurs at 18.0°.

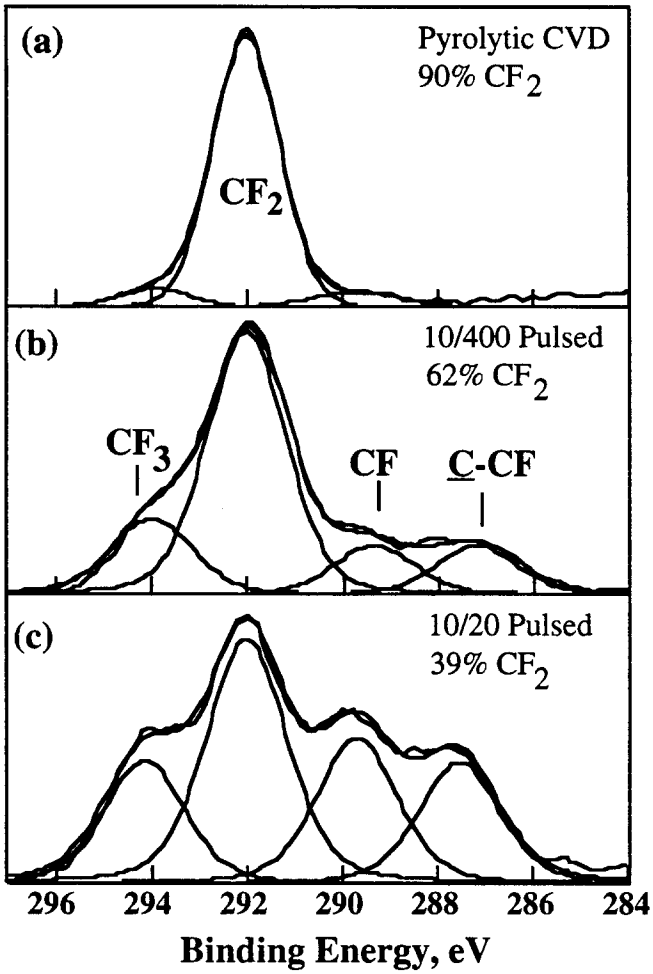

Figure 1.
Macromolecules --Scott J. Limb

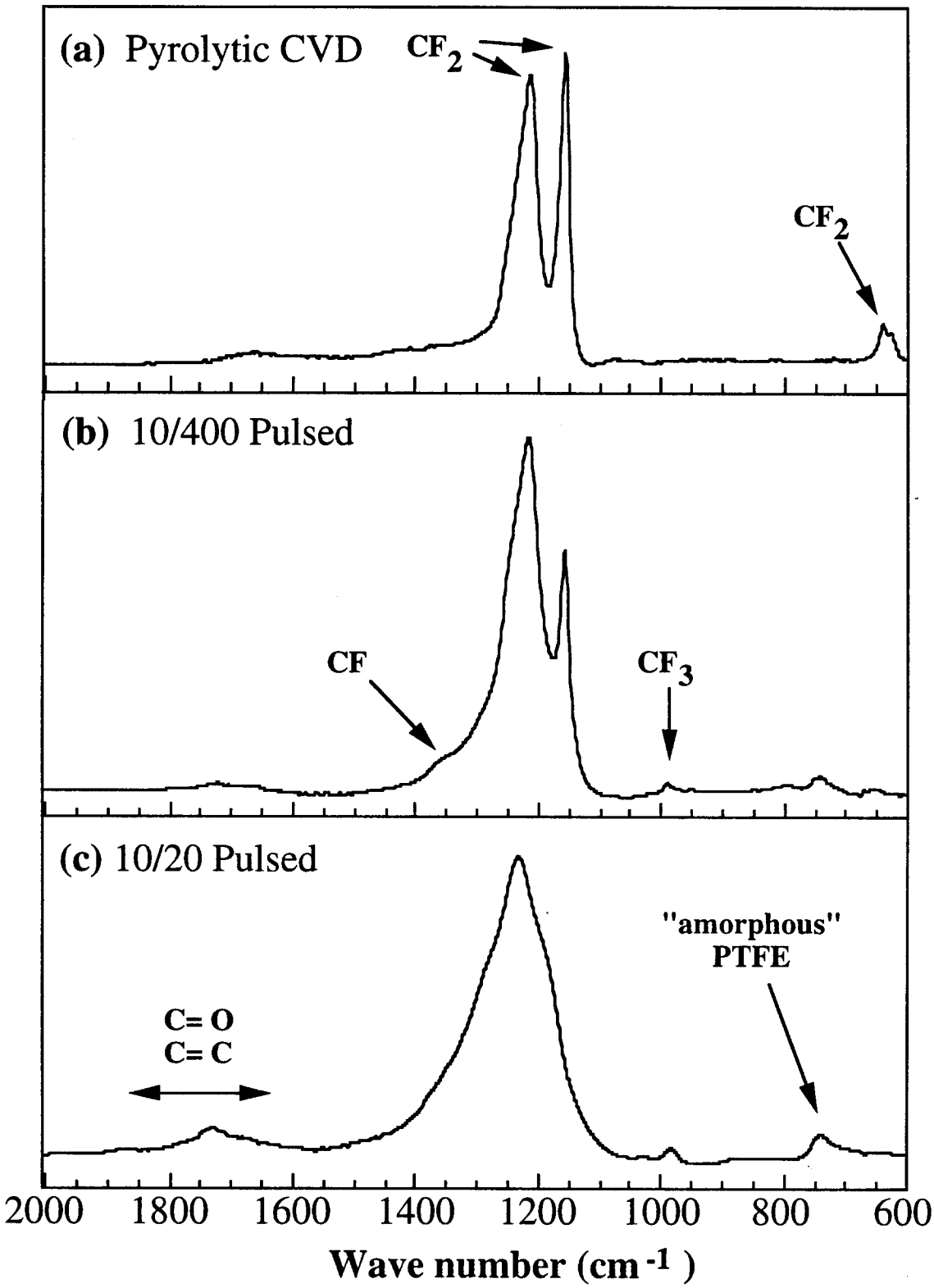

Figure 2.
Macromolecules --Scott J. Limb

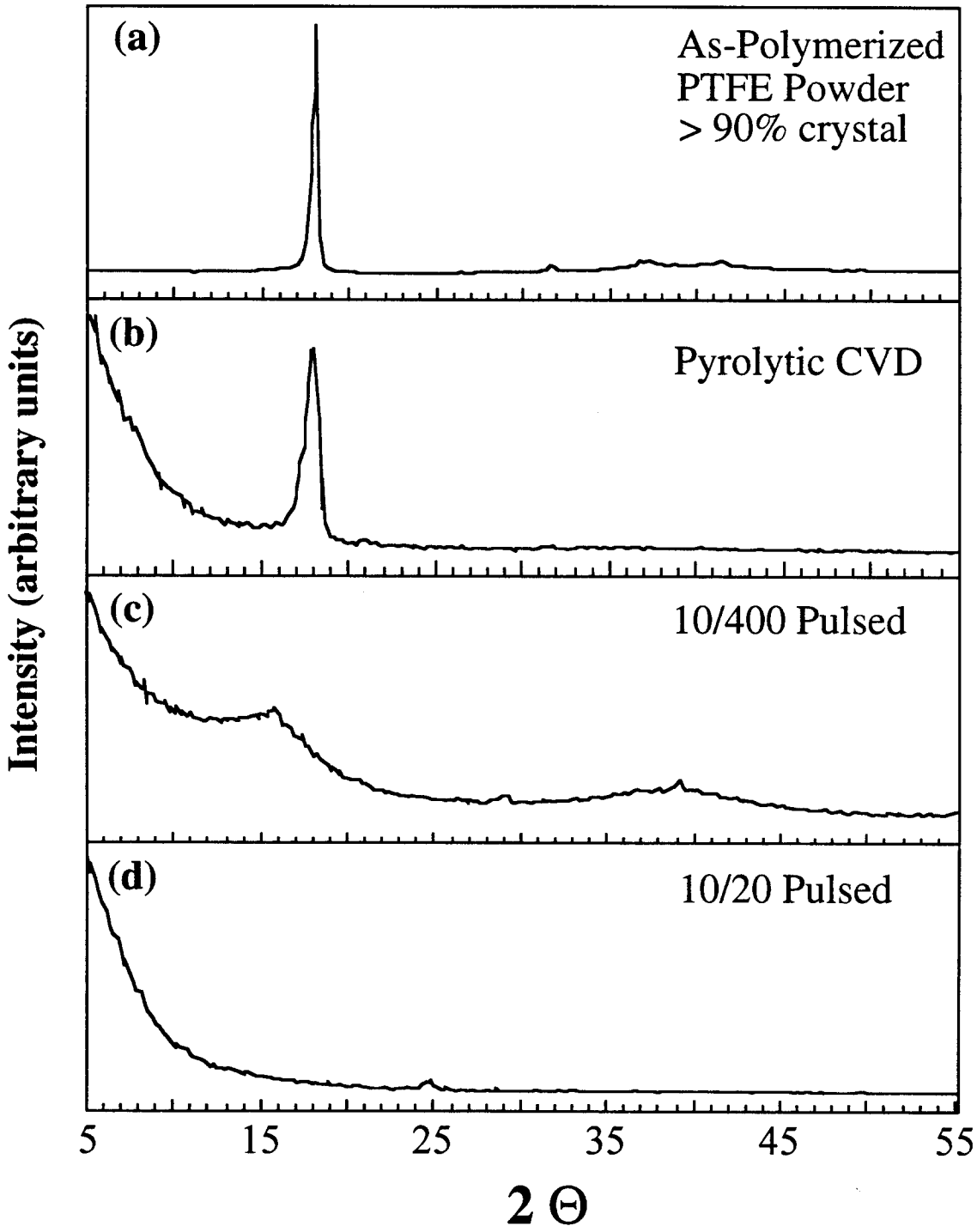

Figure 3.
Macromolecules --Scott J. Limb